We are IntechOpen, the world's leading publisher of Open Access books Built by scientists, for scientists

6,900
Open access books available

185,000
International authors and editors

200M
Downloads

Our authors are among the

154
Countries delivered to

TOP 1%
most cited scientists

12.2%
Contributors from top 500 universities

WEB OF SCIENCE™

Selection of our books indexed in the Book Citation Index in Web of Science™ Core Collection (BKCI)

Interested in publishing with us?
Contact book.department@intechopen.com

Numbers displayed above are based on latest data collected.
For more information visit www.intechopen.com

15

Laser Pulses Applications in Photovoltaic Effect

Kui-juan Jin, Chen Ge, Hui-bin Lu and Guo-zhen Yang
Beijing National Laboratory for Condensed Matter Physics
Institute of Physics, Chinese Academy of Sciences
China

1. Introduction

Laser pulses have been utilized in detecting photovoltaic properties and exploring functional characteristics in the field of solid-state physics (Jain & Landis, 1998; Sun et al., 2004; Lu et al., 2005; Yan et al., 2007; Jin et al., 2009; Lv et al., 2009). Experimental and theoretical investigations into photovoltaic effect under laser pulse are of particular interest for both physics and engineering.

Recent advances in seeking fast photovoltaic response material (Lu et al., 2005; Zhao et al., 2005; Zhao et al., 2006a; Zhao et al., 2006b; Zhao et al., 2006c; Huang et al., 2006), finding one-order-of-magnitude enhancement of lateral photovoltaic (LPV) effect in the perovskite oxide heterostructures compared with the substrates (Jin et al., 2007; Jin et al., 2009), and investigating the dependence of the photovoltaic effect on the thin films and substrates thickness (Qiu et al., 2007; Wen et al., 2009), are attributed to laser pulses applications in the photovoltaic effect. Several years ago, transient photoelectric effects were observed in $La_{0.7}Sr_{0.3}MnO_3$ (LSMO3)/Si heterostructure fabricated by pulsed laser deposition (Lu et al., 2005), which offers opportunities for designing new fast photodetectors. Moreover, the unusual LPV, ascribed to the Dember effect (Pankove, 1971) induced by large numbers of photo-generated carriers under laser pulses, was observed in the heterostructures of both $La_{0.9}Sr_{0.1}MnO_3/SrNb_{0.01}Ti_{0.99}O_3$ (LSMO1/SNTO) and LSMO3/Si (Jin et al., 2007; Jin et al., 2009). A one-order-of-magnitude enhancement of the LPV was found (Jin et al., 2009). Furthermore, the dependence of photovoltage on the thin films and substrates thickness was presented. The photovoltage becomes larger with the increase of the LSMO1 film thickness, while the film thickness is less than the depletion layer of the heterostructures. This is ascribed to the increase of the carrier amount of the LSMO1 layer and the enhancement of the built-in electric field in the space-charge region of the LSMO1/SNTO heterostructure (Qiu et al., 2007). Faster photoelectric response was observed in $LaAlO_{3-\delta}$/Si (LAO/Si) heterostructures, and the photoelectric sensitivity was greatly improved by decreasing the thickness of the Si substrates (Wen et al., 2009).

In order to reveal the underlying physical origin and the dynamic process of the photoelectric effect in the oxide heterostructure, time-dependent drift-diffusion model was employed (Liao et al., 2009a, 2009b, 2009c; Liao et al., 2010; Ge et al., 2010). The theoretical calculations showed that the modulation of Sr doping in $La_xSr_{1-x}MnO_3$ is an effective

method to accommodate the sensitivity and the speed of photovoltaic response (Liao et al., 2009a), that a smaller parallel resistance should result in faster photoelectric response (Liao et al., 2009b), and that the photodoping effect mainly occurs in the space-charge region of heterostructure (Liao et al., 2009c). By self-consistent calculations, it was demonstrated that with the increase in irradiated laser pulse energy, the Dember effect plays a more and more important role in LPV. A unified description for conventional LPV and Dember-effect-induced LPV can be obtained within the frame of drift-diffusion model (Liao et al., 2010). Two mechanisms for the great enhancement of LPV in the heterostructures were also presented by self-consistent calculations: the LPV of *p*-type material is larger than that of *n*-type material owing to the larger drift electric field induced in the *p*-type material than that in the *n*-type material; the built-in electric field at the interface between the thin film and substrate can enhance the LPV (Ge et al., 2010). Position-sensitive detectors (PSD) based on LPV are widely applied in various fields (Henry & Livingstone, 2001), and photo-Dember effect can produce THz in semiconductors under laser pulses (Dekorsy et al., 1993; Dekorsy et al., 1996 ; Gu et al., 2002 ; Liu et al., 2006; Tonouchi, 2007; Krotkus, 2010). Thus, such an understanding of the mechanisms for the enhancement of LPV should be helpful in further designing of the structures of PSD and new THz sources.

This chapter is dedicated to give a brief description of the intriguing experiment phenomena and basic theoretical understanding of photovoltaic effect under laser pulse. It will be organized as follows: the first section is an introduction; the second section focuses on the photovoltaic experiments; the third section addresses the theoretical investigations based on the drift-diffusion model, starting with a detailed description of the self-consistent numerical model; conclusions and perspectives are exhibited in the last section.

2. Photovoltaic experiments

Oxide heterostructures have been emerged as a leading topic in condensed-matter physics, since various fascinating phenomena, including high mobility (Ohtomo A. & Hwang H. Y., 2004) or even superconductivity (Reyren et al., 2007) between insulating oxides, were observed in these systems. In well-fabricated oxide heterostructures, a series of photovoltaic experimental results under laser pulses(Lu et al., 2005; Jin et al., 2007; Qiu et al., 2007; Jin et al., 2009; Wen et al., 2009) showed that desirable unusual effects can be observed, and outstanding functional properties can be obtained in these systems. It should provide avenues into understanding the fundamental properties of these systems and designing of new multifunctional devices.

2.1 Transient photoelectric effects

Many efforts have been devoted to explore functional properties under laser irradiation and design new device based on manganese oxide (Zhang et al., 2002; Sun et al., 2004; Lu et al., 2005; Yu & Wang, 2010). In the past few years, we have investigated the photoelectric effects under laser pulses in a variety of oxide heterostructures (Lu et al., 2005; Zhao et al., 2005; Zhao et al., 2006a; Zhao et al., 2006b; Zhao et al., 2006c; Huang et al., 2006; Wen et al., 2009). It was found that the photoelectrical process is in a picosecond or nanosecond order in the oxide heterostructures, which opens up a door for the applications of oxide heterostructures in the optoelectronic detection devices.

LSMO3 thin films, usually recognized as a *p*-type semiconductor, were deposited on *n*-Si substrate by a computer-controlled laser molecular-beam epitaxy (Laser-MBE) system (Yang

et al., 2001). The growing process of thin films was in situ monitored by reflection high-energy electron diffraction (RHEED). The photoelectric behaviours of LSMO3/Si were further investigated using a 1064 nm Nd:YAG laser (pulse width 25 ps) and measured by an oscilloscope of 130 ps rise time (Tektronix® TDS7254B) at ambient temperature. Figure 1 (Lu et al., 2005) shows a typical open-circuit photoelectric pulse when the LSMO3/Si was irradiated by 1064nm pulsed laser. The rise time is about 10 ns and the FWHM is about 12 μs. So as to reduce the influences of the measuring system and the capacitance of the heterostructure, a 0.2 Ω resistance is connected in parallel with the LSMO3/Si heterostructure. As shown in Fig. 2 (Lu et al., 2005), the rise time dramatically reduces to about 210 ps and the FWHM also reduces to about 650 ps. The photovoltaic process can be easily understood as follows. The Hall measurement showed that the hole concentration of LSMO3 is about 3×10^{18} cm^{-3}, while the electron density of Si is about 1×10^{16} cm^{-3}. When the LSMO3 was grown onto the Si substrate, electrons from *n*-type Si leaked out into the *p*-type LSMO3, while holes from *p*-type LSMO3 moved into the *n*-type Si due to the carrier diffusion. The diffusion induced a built-in electric field around the interface in the space charge region. Under the illumination of pulsed laser, the electron-hole pairs were generated, and then quickly separated by the built-in field. Eventually, the photovoltage occurred in the heterostructure. In addition, we observed that the rise time is about 9 ns in $SrTiO_{3-\delta}$/Si heterostructure (Zhao, et al., 2005), 23 ns in LSMO1/SNTO heterostructure (Huang et al., 2006) and 86 ps in $LaAlO_{3-\delta}$/Si (Wen et al., 2009).

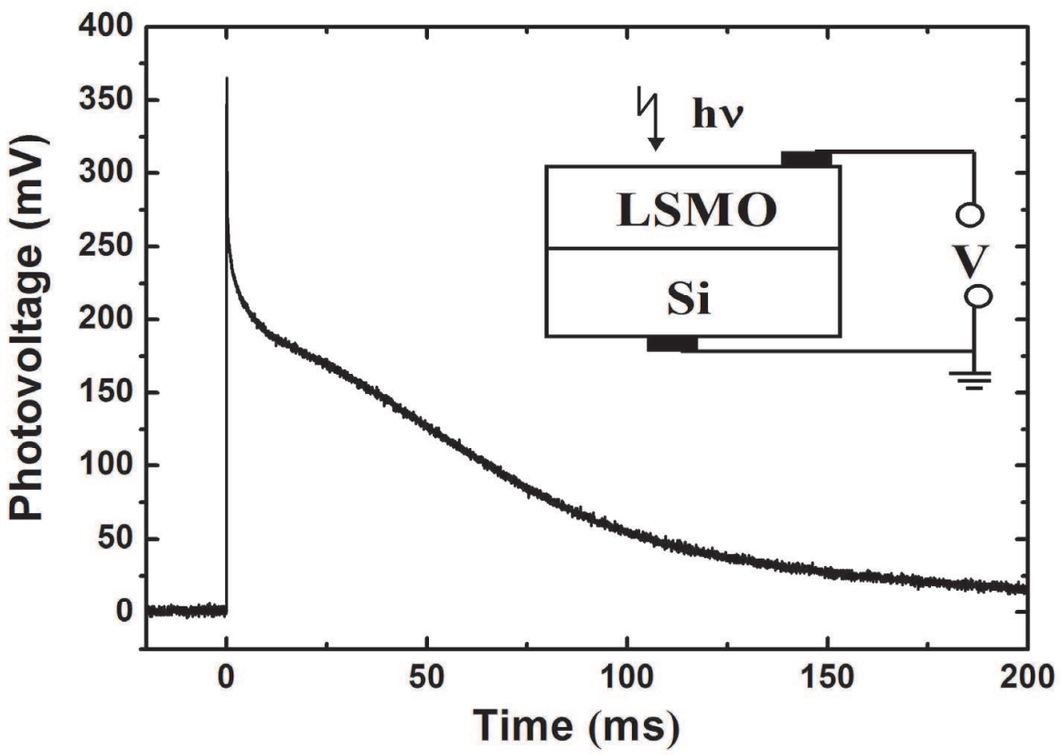

Fig. 1. Variation of the open-circuit photovoltage with time after excitation with a 1064 nm laser pulse on the LSMO3/Si. The schematic circuit of the sample measurement is shown in the inset.

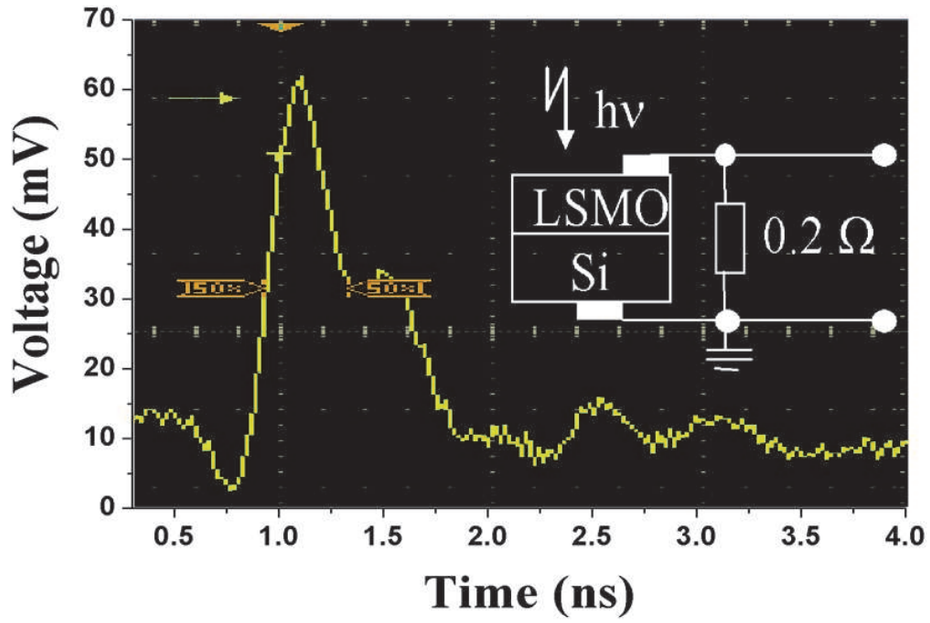

Fig. 2. Variation of the photovoltage with time under the same condition as in Fig. 1, but with a 0.2 Ω resistance connected in parallel across the heterostructure. Inset displays a schematic circuit of the sample measurement.

2.2 Enhancement of lateral photovoltage in oxide heterostructures

As stated above, all these works about ultrafast photoelectric effects focused on the photovoltaic effect across the oxides heterostructures. Furthermore, LPV experiments under the illumination of pulsed laser were also carried in order to further study the photovoltaic effect in oxides heterostructures (Jin et al., 2007; Jin et al., 2009). The well-established LPV theory (Wallmark, 1957; Lucovsky, 1960), that in nonuniformly irradiated *p-n* junctions electric potential near the irradiation center is higher than that far from the center on the *p*-type side while it is lower than that far away from the center on the *n*-type side, was challenged by the observed unusual LPV (Jin et al., 2007). In other words, the signs measured on both sides of *p-n* junction will be opposite according to the conventional LPV whereas they are same in the observed unusual LPV. Therefore, Dember effect (Pankove, 1971), induced by the different mobility of photogenerated electrons and holes, was introduced to qualitatively explain the unusual LPV in the oxide heterostructures (Jin et al., 2007).

LSMO1/SNTO and LSMO3/Si heterostructures were fabricated by growing a *p*-type LSMO1 (LSMO3) layer on a *n*-type SNTO (Si) substrate, with the computer-controlled laser-MBE technique. The schematic setup for LPV measurements is shown in the insets of Figure 3. A small area of 0.5 mm diameter on the *p*-LSMO surface was illuminated by a 308 nm XeCl excimer laser beam (pulse width of 20 ns, pulse energy of 0.15 mJ, and repetition rate of one pulse every 5 min to avoid the heating effect). We moved the samples in the lateral direction and recorded the LPV values, by a sampling oscilloscope of 500 MHz terminated into 1 MΩ at room temperature. Here, the photovoltage, which denotes the peak value of the LPV between the indium electrodes A (x = -3 mm) and B (x = 3 mm) on the LSMO1 (LSMO3) surface, depends on the laser spot position in the LSMO1/SNTO (LSMO3/Si)

heterostructure. In addition, the diameter of indium electrodes is about 1 mm. Particularly, the electrodes were always kept in dark to prevent any electrical contact effects.

Figure 3(a) (Jin et al., 2009) exhibits the measured LPV values in LSMO1/SNTO heterostructure. Figure 3(b) (Jin et al., 2009) depicts the experimental LPV values in LSMO3/Si heterostructure. From Fig. 3(a) and Fig. 3(b), it can be seen that the signs of LPV are same on both sides of heterostructures. This phenomenon can be explained as follows. As both electrons and holes are induced by photons and flow out on two sides of oxide heterostructures, the mobility difference of electrons and holes causes the same sign (positive or negative) of LPV on both sides of oxide heterostructures. It should be noted that only strong light can make the Dember-effect-induced LPV large enough to be observed. To compare the LPV in the heterostructures and that in substrates, the LPV measurements for *n*-SNTO and *n*-Si substrates were also carried out and the results are shown in Fig. 3(c) (Jin et al., 2009). Evidently, it can be concluded that a one-order-of-magnitude enhancement of the LPVs was observed, as compared with those of the substrates.

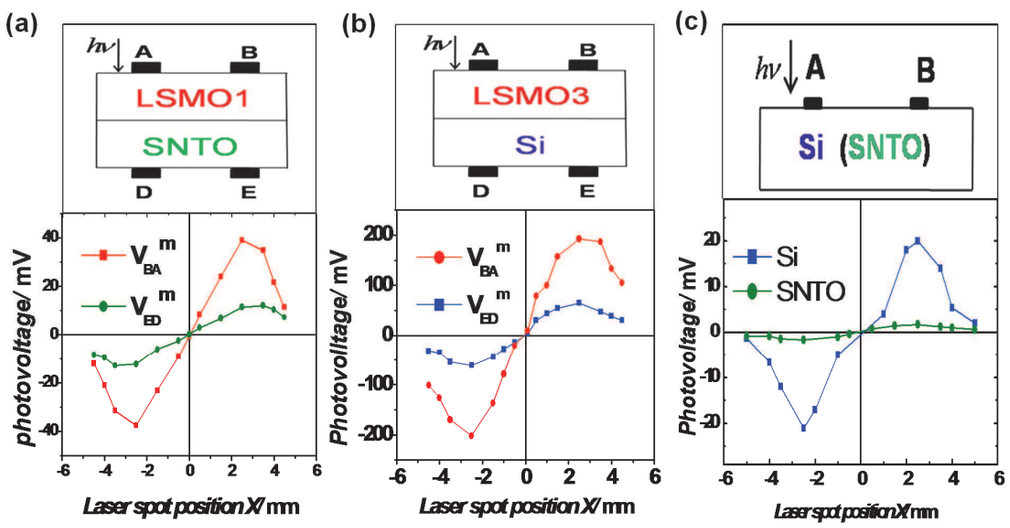

Fig. 3. The peak values of LPV V_{BA}^{m} and V_{ED}^{m} as a function of the position of the laser spot in the x direction in (a) the LSMO1/SNTO and in (b) LSMO3/Si heterostructures, the upper panel displays the schematic setup for the LPV measurement. A (–3 mm), B (3 mm), D (–3 mm), and E (3 mm) denote the electrodes. (c) The peak values of LPV, V_{BA}^{m}, for *n*-SNTO (open triangles) and Si (open squares) substrates.

In fact, it is well known that the optical generation of THz radiation can be produced in the conventional semiconductors using the photo-Dember effect under ultra-short pulse laser illumination (Dekorsy et al., 1993; Dekorsy et al., 1996; Gu et al., 2002; Liu et al., 2006; Tonouchi, 2007; Krotkus, 2010). Thus, the understanding of the underlying physical mechanisms for such an enhancement is fundamentally important and should be of great value for the further designing of the structures of potential applications in powerful THz sources. Mechanisms for the enhancement of LPV in oxide heterostructures will be discussed in detail later.

2.3 Dependence of photovoltage on the films and substrates thickness

For LPV effect, a one-order-of-magnitude enhancement of photovoltage can be obtained in oxide heterostructures compared with that of substrates. Then, to find out how to improve the sensitivity of photovoltaic effect across the heterostructures, surveys on the dependence of photovoltage on the films and substrates thickness were systematically carried out (Qiu et al., 2007; Wen et al., 2009).

A series of LSMO1/SNTO heterostructures with various films thickness were fabricated by Laser-MBE, for investigating the dependence of photovoltage on the films thickness. The growing process of LSMO1 layers was in situ monitored by RHEED. One period in the RHEED intensity oscillations marks the completion of one unit cell. Hence the thickness of LSMO1 ultrathin films was accurately controlled by the growth time which represented the number of the periods of the RHEED intensity oscillations.

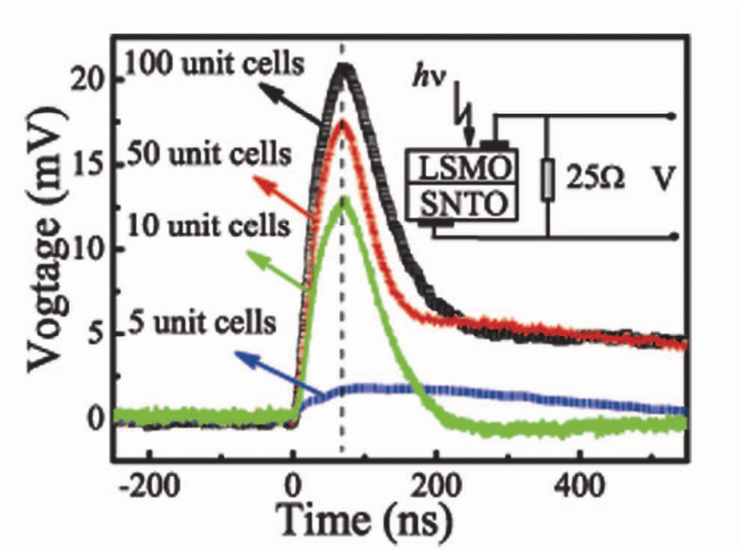

Fig. 4. The open-circuit photovoltage as a function of time to LSMO1/SNTO heterostructures. The inset presents the schematics of the measurement circuit.

Figure 4 shows that the maximum open-circuit photovoltage was about 2, 13, 17 and 21mV for the LSMO1/SNTO heterostructures with LSMO1 thicknesses of 20, 40, 200 and 400Å, respectively. The photovoltage becomes larger with the increase of the thickness of the LSMO1 layer. This result is ascribed to the increase of the carrier amount and the enhancement of the built-in electric field in the space-charge region of the LSMO1/SNTO heterostructure with the increase of the thickness of LSMO1 layer (Qiu et al., 2007). However, it is found that the speed of photovoltaic response is almost independent of the thickness of LSMO1 layer in the heterostructure. It should be useful to comprehend the photovoltaic characteristics in complex oxides materials.

Not only the thickness of films but also the thickness of the substrates can remarkably affect the photoelectric properties of oxide heterostructures. The 400 nm LAO thin films were epitaxially grown on *p*-type Si substrates (thickness 0.71 mm) by a computer controlled Laser-MBE system using two-step method (Wen et al., 2009). Then, three pieces of Si substrates will be polished mechanically until the thickness is 0.44, 0.19, and 0.10 mm, respectively. For convenience, the four samples of various substrate thicknesses will be

denoted as F1 (0.71 mm) F2 (0.44 mm) F3 (0.19 mm) and F4 (0.10 mm) respectively. For the photovoltaic measurements, two indium electrodes were painted on the surfaces of LAO film and Si substrate. During the measurements, the electrodes were always kept in the dark to prevent the generation of any electrical contact photovoltage. All of the photoelectric measurements were carried out at room temperature.

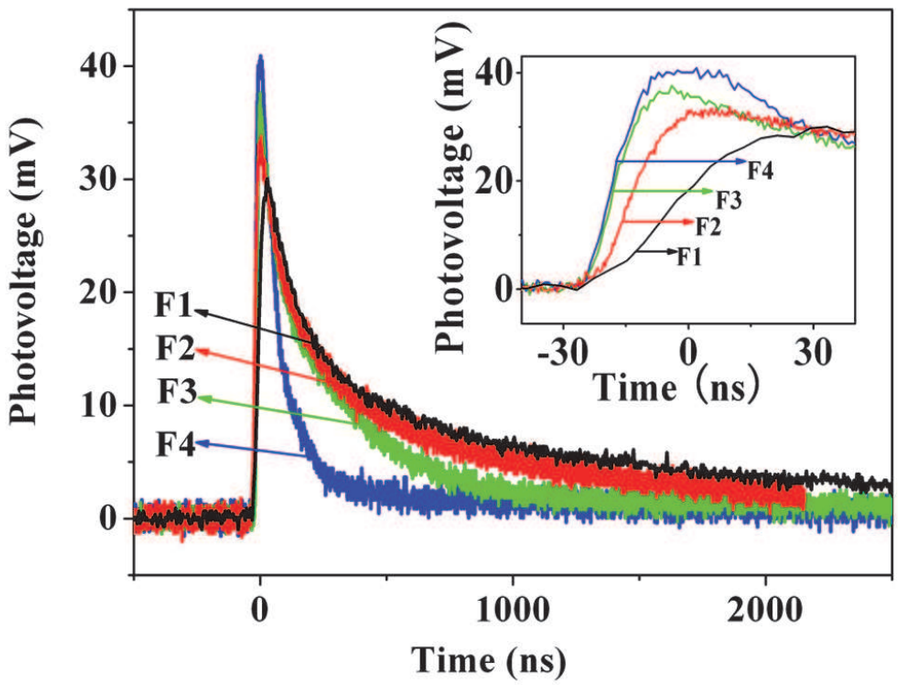

Fig. 5. The photovoltaic responses of LAO/Si heterostructures under the illumination of XeCl pulsed laser for samples F1, F2, F3, and F4. The inset is the rise time of photovoltaic response.

The influence of substrate thickness on photoelectrical effects of LAO/Si heterostructure was systematically investigated on samples F1, F2, F3, and F4 by a 308 nm XeCl excimer pulsed laser (pulse width 20 ns and energy density 0.1 J/cm^2) with a laser spot diameter of 2 mm. Figure 5 shows the dependence of the photovoltaic response on the substrate thickness. The photovoltaic signals were measured by an oscilloscope with 500 MHz bandwidth and an input impedance of 50 Ω. For the four samples F4, F3, F2, and F1, the 10%–90% rise times were 13.3, 13.9, 21.4, and 38.3 ns, respectively, and the FWHMs were 79.2, 134.7, 180.6, and 258.2 ns, respectively. The rise time of the photoelectric signal is faster for the heterostructure with thinner substrate. Meanwhile, the FWHM decreases with the decrease in substrate thickness. It can be understood in the following way: photogenerated carriers were separated by built-in electric field at the interface between LAO and Si, and those holes reached the surface of the substrate faster for thinner substrate so that faster photoelectric response can be observed. Smaller FWHM for the heterostructure with thinner substrate can be understood in the similar way. Overall, the decrease in the substrate thickness is an effective method for improving the photovoltaic sensitivity in oxide heterostructures.

3. Theoretical investigations

Photovoltaic experiments exhibit attractive properties and interesting phenomena in oxide heterostructures under the illumination of pulsed laser as mentioned above. Although several qualitative explanations were proposed, it is rather significant to further quantitatively clarify the physical origins and underlying mechanisms. It is therefore necessary to carry out self-consistent calculations based on the time-dependent drift-diffusion model.

3.1 Time-dependent drift-diffusion model

3.1.1 One-dimensional drift-diffusion model

Self-consistent calculation of drift-diffusion model, first proposed by Scharfetter and Gummel (Scharfetter & Gummel, 1969), is a powerful and effective method of describing carrier transport behaviour in semiconductor devices and is still widely used today(Grasser et al., 2003). In oxide heterostructures, some early theoretical works confirmed that numerical calculations based on drift-diffusion model could be employed to depict not only the steady transport behaviour (Zhou et al., 2005; Han et al., 2007; Hu et al., 2008; Hu et al., 2009) but also the transient transport behaviour (Liao et al., 2009a, 2009b, 2009c; Liao et al., 2010; Ge et al., 2010). One-dimensional time-dependent drift-diffusion model consists of the Poisson equation and carrier continuity equations as follows:

$$\frac{\partial^2 \phi(x,t)}{\partial x^2} = -\frac{e}{\varepsilon}[p(x,t) - n(x,t) + N] \tag{1}$$

$$\frac{\partial n(x,t)}{\partial x} = \frac{1}{e}\frac{\partial j_n(x,t)}{\partial x} + G(x,t) - R(x,t) \tag{2}$$

$$\frac{\partial p(x,t)}{\partial t} = -\frac{1}{e}\frac{\partial j_p(x,t)}{\partial x} + G(x,t) - R(x,t) \tag{3}$$

$$j_n(x,t) = -e\mu_n n(x,t)\frac{\partial \phi(x,t)}{\partial x} + kT\mu_n \frac{\partial n(x,t)}{\partial x} \tag{4}$$

$$j_p(x,t) = -e\mu_p p(x,t)\frac{\partial \phi(x,t)}{\partial x} - kT\mu_p \frac{\partial p(x,t)}{\partial x} \tag{5}$$

Where $\phi(x,t)$, $n(x,t)$ and $p(x,t)$ denote electrostatic potential, electron and hole densities; x and t is position and time coordinates; e, ε and N is electron charge, dielectric permittivity, net ionized impurity densities, respectively; $j_n(x,t)$ and $j_p(x,t)$ denote the electron and hole current densities respectively; μ_n and μ_p represent electron and hole mobility respectively. k and T represent Boltzmann constant and temperature taken as room temperature. The electron-hole pairs generation rate $G(x,t)$ can be expressed as $G(x,t) = I_0(t)\alpha\beta\exp(-\alpha x)$, where $I_0(t)$, α and β denote the density of incident photon flux, absorption coefficient and quantum efficiency. $R(x,t)$ denotes the recombination rate, here presented by the Shockley-Read-Hall (SRH) model (Shockley & Read, 1952). The interface condition for solving the Poisson equation Eq. (1) is taken as $\phi(x_{inter} - \delta, t) = \phi(x_{inter} + \delta, t)$, where x_{inter} denotes the position of the interface and δ is

infinitesimal. At the interface of heterostructures, the Richardson thermionic emission current is employed as interface conditions (Yang et al., 1993) for solving Eq. (2) and (3). The initial values $\phi(x,0)$, $n(x,0)$ and $p(x,0)$ for self-consistent calculations were obtained by solving the Poisson equation coupled with the Boltzmann approximation (Selberherr, 1984).

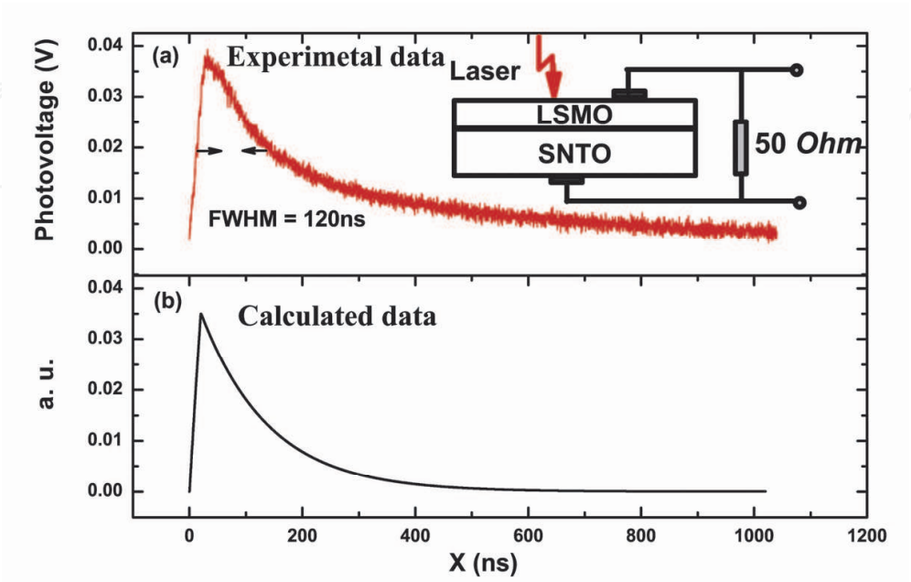

Fig. 6. (a) Experimental evolution of photovoltage in the LSMO1/SNTO heterostructure connected with 50 Ω resistance. The inset presents the illustration of heterostructure for voltaic measurement. (b) The calculated evolution of photovoltage.

The dependence of photovoltaic response on the time is shown in Fig. 6 (a) (Liao et al., 2009c) in LSMO1/SNTO heterostructure irradiated by a XeCl pulsed laser (wavelength of 308 nm, repetition rate of 1 Hz and duration of 20 ns). The inset in Fig. 6 presents the illustration of heterostructure for photovoltaic measurement. Figure 6 (b) shows the numerical result by self-consistently solving Eq. (1)-(5). The necessary parameters for numerical calculations are listed in Table 1. More details about the experiment and calculation can be found in Ref. Liao et al., 2009c. Apparently, the theoretical results are in good agreement with the experimental data in LSMO1/SNTO. Consequently, it can be concluded that the time-dependent drift-diffusion model can also well describe the transient transport of the oxide heterostructures.

On the basis of the good numerical simulations, the dependence of transient photovoltaic response on the various physical parameters was further analyzed (Liao et al., 2009a, 2009b, 2009c), which could be useful to the future experimental investigations on the photovoltaic properties of oxide heterostructures irradiated by pulsed laser. The theoretical caculations represented that the modulation of Sr doping in $La_xSr_{1-x}MnO_3$ is an effective method to accommodate the sensitivity and the speed of photovoltaic response (Liao et al., 2009a), that a smaller parallel resistance should result in faster photoelectric response and the increase of the carrier mobilities induced by applying higher energy photons can decrease the rise time but increase the peak value of the photovoltage (Liao et al., 2009b), and that the large variation of carrier concentration mainly locates in the space-charge region of the oxide heterostructure (Liao et al., 2009c).

	LSMO1(3)	SNTO	Si
Temperature (K)	300	300	300
Dielectric constant(ε_0)	10.0	300.0	11.9
Electron mobility ($cm^2/(V.s)$)	10.0	8.0	1450
Hole mobility ($cm^2/(V.s)$)	1.8	0.1	500
Band gap (eV)	0.8	2.8	1.12
Ionized impurity concentrations ($/cm^3$)	$4.0\times10^{19}(1.0\times10^{20})$	1.63×10^{20}	1.0×10^{17}
Photon absorption coefficient(cm^{-1})	1.5×10^5	1.2×10^5	4×10^5

Table 1. The parameters for self-consistent calculations. (Ge et al., 2010, and references therein)

3.1.2 Two-dimensional drift-diffusion model

As mentioned above, the further theoretical analysis of unusual LPV phenomenon and great enhancement of LPV is fundamentally important in terms of both physics and engineering. A quantitative approach was thereby introduced based on two-dimensional time-dependent drift-diffusion model (Liao et al., 2010; Ge et al., 2010). The equations are as follows:

$$\frac{\partial^2\phi(x,y,t)}{\partial x^2}+\frac{\partial^2\phi(x,y,t)}{\partial y^2}=-\frac{e}{\varepsilon}[p(x,y,t)-n(x,y,t)+N] \tag{6}$$

$$\frac{\partial n(x,y,t)}{\partial t}=\frac{1}{e}\nabla\cdot\vec{j}_n(x,y,t)+G(x,y,t)-R(x,y,t) \tag{7}$$

$$\frac{\partial p(x,y,t)}{\partial t}=-\frac{1}{e}\nabla\cdot\vec{j}_p(x,y,t)+G(x,y,t)-R(x,y,t) \tag{8}$$

$$\begin{aligned}\vec{j}_n(x,y,t)=&[-e\mu_n n(x,y,t)\frac{\partial\phi(x,y,t)}{\partial x}+eD_n\frac{\partial n(x,y,t)}{\partial x}]\cdot\boldsymbol{i}_x\\&+[-e\mu_n n(x,y,t)\frac{\partial\phi(x,y,t)}{\partial y}+eD_n\frac{\partial n(x,y,t)}{\partial y}]\cdot\boldsymbol{i}_y\end{aligned} \tag{9}$$

$$\begin{aligned}\vec{j}_p(x,y,t)=&[-e\mu_p p(x,y,t)\frac{\partial\phi(x,y,t)}{\partial x}-eD_p\frac{\partial p(x,y,t)}{\partial x}]\cdot\boldsymbol{i}_x\\&+[-e\mu_p p(x,y,t)\frac{\partial\phi(x,y,t)}{\partial y}-eD_p\frac{\partial p(x,y,t)}{\partial y}]\cdot\boldsymbol{i}_y\end{aligned} \tag{10}$$

where x and y denote the transverse and lateral axes, respectively, and i_x and i_y are the unit vectors along the x and y axes, respectively. Similar to the one-dimensional drift-diffusion model, all the symbols denote the same physical quantities. $G(x,y,t)$ is the generation rate of the photoinduced electron-hole pairs, expressed as $G(x,y,t)=I_0(y,t)\alpha\beta\exp(-\alpha x)$, where α and β denote the absorption coefficient and quantum efficiency respectively. $I_0(y,t)$ denotes the incident photon flux density. Furthermore, in our calculations, $I_0(y,t)$ is considered as a Gauss distribution function. Actually, Eqs. (6)-(10) are rather difficult to be solved. Owing to the large difference in the scale between the two dimensions, width and

the thickness, a huge rounding error is caused in the numerical calculation of Poisson equations. For solving this problem, we decompose the Poisson equation Eq. (6) into two following independent equations:

$$\frac{\partial^2 \phi_x(x,y,t)}{\partial x^2} = Q_x(x,y,t) \tag{11}$$

$$\frac{\partial^2 \phi_y(x,y,t)}{\partial y^2} = Q_y(x,y,t) \tag{12}$$

where $Q_x(x,y,t)$ and $Q_y(x,y,t)$ represent the charge densities in transverse and lateral direction, respectively, $\phi_x(x,y,t)$ and $\phi_y(x,y,t)$ denote the electric potential distributions excited by the charge in transverse and lateral direction, respectively. The total potential distribution is $\phi(x,y,t) = \phi_x(x,y,t) + \phi_y(x,y,t)$. The two-dimensional continuity equations can also be decomposed into two groups of one-dimensional equations. These equations can be solved on the basis of the self-consistent calculations of transverse photovoltaic effect stated above (Liao et al., 2009a, 2009b, 2009c). More details of numerical calculations can be found in Ref. Liao et al., 2010.

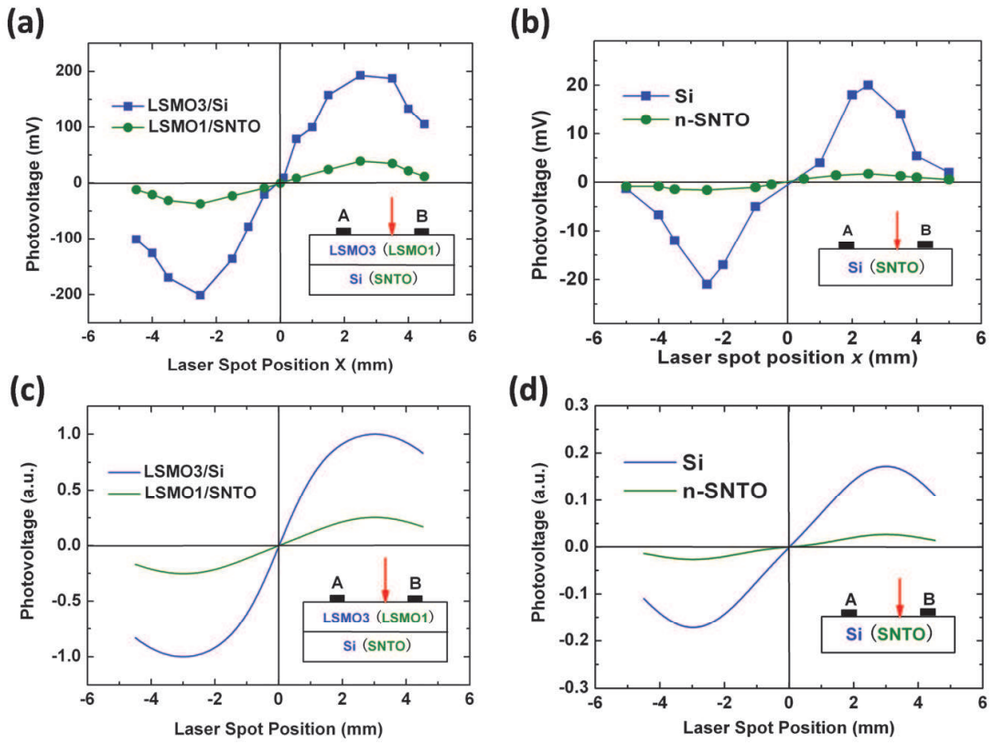

Fig. 7. The experimental (a) and theoretical (c) LPVs of the LSMO side in the LSMO1/SNTO denoted by the green curve and LSMO3/Si denoted by the blue curve; the experimental (b) and theoretical (d) LPVs of SNTO denoted by the green curve and Si denoted by the blue curve. The photovoltage denotes the peak value of LPV between the indium electrodes A (x = −3 mm) and B (x = 3 mm). The inset shows the schematic setup for LPV measurement.

Figure 7 (a) (Jin et al., 2007, 2009) exhibits the experimental LPVs of LSMO side in the LSMO1/SNTO (the green circular curve) and LSMO3/Si (the blue square curve) heterostructures. Figure 7 (b) (Jin et al., 2009) depicts the experimental LPVs of SNTO (the green circular curve) and Si (the blue square curve) substrates. Our calculated results for LPVs on the LSMO side in LSMO1/SNTO and LSMO3/Si heterostructures are shown in Fig. 7 (c) (Ge et al., 2010) as the green curve and blue one, respectively. The calculated LPVs on SNTO and Si substrates are displayed in Fig. 7 (d) (Ge et al., 2010) by the green curve and the blue curve, respectively. The necessary parameters for the calculations are listed in Table 1 (Ge et al., 2010). We use a.u. to show our calculated results to compare with the experimental data in the curves, due to the fact that our model purely describes the charge contribution in the heterostructure and the experimental data includes more complicated factors in the measuring circuit, contacts, and so on. It can be seen that the calculated results are in good accordance with the experimental data. Then a much clearer insight into the unusual LPV and one-order-enhancement of LPV can be obtained from the present calculations.

3.2 Theoretical discussion based on self-consistent calculations

3.2.1 Unified descriptions of the conventional and unusual LPV

So as to find out the reasons that the unusual LPV differs from the conventional LPV considerably, we carried out a throughout investigation of the dependence of LPV on the laser pulse energy.

As shown in Fig. 8 (a) (Liao et al., 2010), the calculated values of the electric potential on the LSMO1 side turn to be larger and larger with the increase in laser pulse energy. The trends of electric potential distribution on the two sides of the heterostructure are opposite to each other under the laser pulse energy lower than 0.015 mJ, while they turn to be the same with each other under the laser pulse energy higher than 0.015 mJ. As shown in Fig. 8 (d) (Liao et al., 2010), the corresponding calculated LPV on the SNTO side exhibits laterally modulated behaviours under the laser pulse energy of 0.015 mJ, while calculated LPV on the LSMO1 side becomes larger and larger with the increase in laser pulse energy as shown in Fig. 8 (c) (Liao et al., 2010). This laterally modulated LPV effect can be explained by the competition between Dember and conventional LPV processes.

Under critical laser pulse energy, the conventional LPV effect and the Dember effect are comparable to each other. Hence, neither of them can dominate the LPV all over the region. In the region near the irradiation center (-2.0 mm, 2.0 mm) where the carrier density is high due to the strong laser pulse irradiation, the Dember effect is stronger than the conventional LPV effect, as shown in Fig. 8. Therefore, in this region, the farther the position is away from the irradiation center, the smaller electric potentials are on both sides. While in the region far away from the irradiation center (2.0 mm, 7.5 mm) and (-7.5 mm, 2.0 mm) where the carrier density is low, the Dember potential is weak, as shown in Fig. 8. As a result, the conventional LPV effect is the main contributor to the LPV. Thus, our calculated results unified the description of the conventional LPV and the Dember effect into the drift-diffusion model.

The evolution and the competition process of the conventional and Dember LPV effect have been revealed theoretically. With the increase in irradiated laser pulse energy, the Dember effect plays a more and more important role in lateral photovoltaic effect. In conclusion, the laser pulse energy is the key factor in determining whether the conventional or the Dember LPV effect dominate the LPV. The corresponding experiments are highly expected.

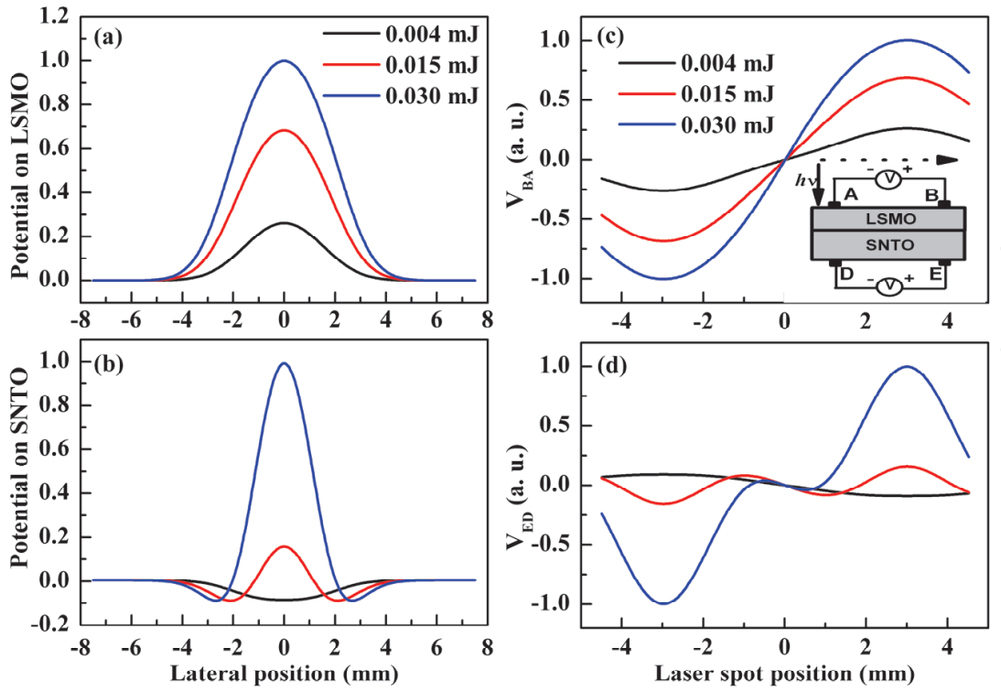

Fig. 8. The electric potential distributions near the irradiation center of the LSMO1/SNTO heterostructure with varied irradiation laser pulse energies (0.004, 0.015, 0.030 mJ) (a) on the LSMO1 side and (b) on the SNTO side. The calculated LPVs of the LSMO1/SNTO heterostructure with varied irradiation laser pulse energies (0.004, 0.015, and 0.030 mJ) (c) on the LSMO1 side and (d) on the SNTO side. The inset in Fig. 8 (c) shows the schematic setup for LPV measurement.

3.2.2 Mechanisms for the great enhancement of LPV

From the above calculations, the mechanisms for the one-order-of-magnitude enhancement of the Dember-effect-induced LPV can be revealed. There are mainly two physical origins. Firstly, we find that the Dember-effect-induced LPV of the *p* type material is larger than that of the *n* type material with the same carrier concentration. As illustrated in Fig. 9 (a) (Ge et al., 2010), we calculated the Dember-effect-induced LPVs of the *p* type material and *n* type material with the same carrier concentration of 1×10^{17} cm^{-3}. It can be seen that the LPV of the *p* type material is almost twice as large as that of the *n* type material. This can be totally ascribed to the difference between the mobilities of electrons and holes. The amounts of photo-generated electrons and holes are the same in both the *p* type material and *n* type material under the same condition. Consequently, the lateral diffusion current densities are the same. However, the main drift carriers for *p* type material are holes, while the main drift carriers for *n* type material are electrons. Assuming that the system is in the steady state that the drift current densities can just balance the diffusion current densities, the lateral drift current densities are of the same value for the *p* type material and *n* type material. Thus, the drift electric field of the *p* type material should be larger than that of the *n* type material, as the mobility of holes is smaller than that of electrons. Hence, it can be concluded that the Dember-effect-induced LPV of the *p* type material is larger than that of the *n* type material. Moreover, the Dember-effect-induced THz radiation from the surface of *p*-InAs wafer has

been reported as a strong THz emitter (Tonouchi, 2007; Krotkus, 2010). We believe that the present study gives an insight into the physical origin of such an application.

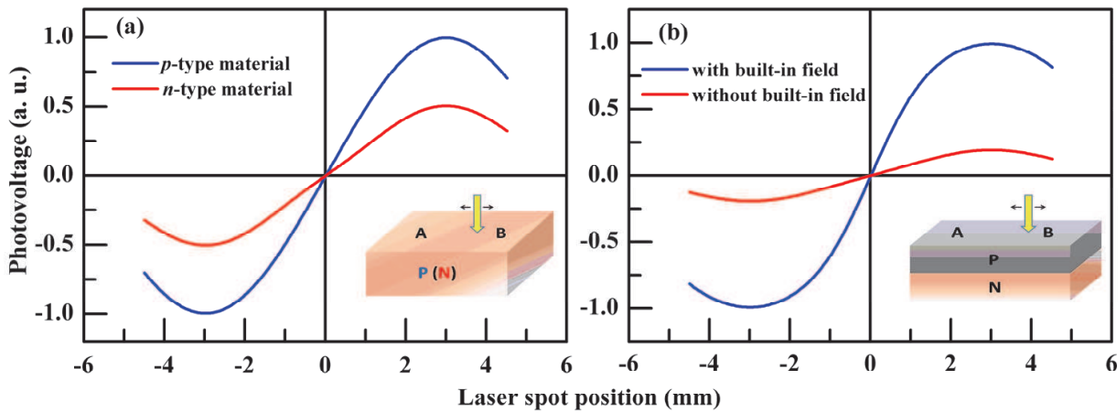

Fig. 9. (a) The calculated LPVs between the electrodes A (x = −3 mm) and B (x = 3 mm) in the same material with different doping type. The blue and red curves denote the LPVs in the *p*-type and *n*-type material, respectively. The inset exhibits the schematic setup. (b) The blue and red curves denote the calculated LPVs between the electrodes A (x = −3 mm) and B (x = 3 mm) in the same heterostructures with built-in field and without built-in field, respectively. The lower inset exhibits the schematic setup.

Secondly, from our calculations we find that the built-in electric field at the interface between the thin film and the substrate also plays an important role in the LPV effect. For revealing the influence of the built-in electric field, we assumed that the potential difference between the *p* type region and the *n* type region was zero and 0.52 Volt for the structure without and with the built-in electric field in our self-consistent calculations, respectively. Figure 9 (b) (Ge et al., 2010) shows the calculated LPVs for the heterostructure with and without the built-in electric field denoted by the blue curve and the red curve, respectively. From Fig. 9 (b), it can be estimated that the heterostructure with a small built-in field of 0.52 Volt can produce a five times larger LPV than that of the heterostructure without the built-in field. For the structure with the built-in electric field, the photo-generated electron-hole pairs can be separated by the built-in electric field. Thereby, the photo-generated holes are swept into the *p* type layer, and the potential of the irradiation region is raised relative to the situation without the built-in electric field. As a result, the Dember-effect-induced LPV for the structure with the built-in electric field is enhanced compared to the one without the built-in electric field. The combination of the above two mechanisms can well explain the one-order-of-magnitude enhancement of the LPV in the oxide heterostructures compared with that in the substrates.

The understanding of the mechanisms for the enhanced LPV in oxide heterostructures should be useful in further designing of the structures of potential applications in novel functional devices, for instance high sensitive PSDs and powerful THz sources.

4. Conclusion and outlook

In conclusion, we have sought to give a brief description of currently most important applications of laser pulses in photovoltaic effect. Fast transient photoelectric effects were observed in LSMO3/Si heterostructure fabricated by pulsed laser deposition technique,

which opens up possibilities to design new photodetectors based on oxides. Furthermore, the unusual LPV was observed in the heterostructures of both LSMO1/SNTO and LSMO3/Si. Then, a one-order-of-magnitude enhancement of the LPV was found. Moreover, the dependence of photovoltage on the thin films and substrates thickness was elaborated. The photovoltage becomes larger with the increase of the LSMO1 film thickness, while the film thickness is less than the depletion layer of the heterostructures. This is attributed to the increase of the carrier amount of the LSMO1 layer and the enhancement of the built-in electric field in the space-charge region of the LSMO1/SNTO heterostructure. Faster photoelectric response was observed in LAO/Si heterostructure, and the photoelectric sensitivity was greatly improved by decreasing the thickness of the Si substrates.

To give much insight into the underlying physical origins of the fascinating phenomena under laser pulses, theoretical investigations were carried out on the basis of the time-dependent drift-diffusion model. The theoretical calculations of one-dimensional drift-diffusion model proved that the modulation of Sr doping in $La_xSr_{1-x}MnO_3$ is an effective method to accommodate the sensitivity and the speed of photovoltaic response, that a smaller parallel resistance should result in faster photoelectric response, and that the photodoping effect mainly occurs in the space-charge region. By self-consistent calculations, it can be seen that with the increase in irradiated laser pulse energy, the Dember effect plays a more and more important role in LPV. A unified description for conventional LPV and Dember-effect-induced LPV can be achieved within the frame of drift-diffusion model. The two mechanisms for the great enhancement of LPV in the heterostructures were also presented by self-consistent calculations: the LPV of *p*-type material is larger than that of *n*-type material owing to the larger drift electric field induced in the *p*-type material than that in the *n*-type material; the built-in electric field at the interface between the thin film and substrate can enhance the LPV. Such an understanding of the mechanisms for the enhancement of LPV should be helpful in further designing of the structures of PSD and new THz sources.

The comparison of the theoretical results presented in this chapter with various experimental data and their satisfactory agreement are evidences that the proposed model and the results obtained on its basis are sufficiently accurate and reliable. The methods and approaches presented can be used for the further development of new approaches of laser pulse applications in photovoltaic effect. Currently, there are still a large number of open questions in this filed. For instance, novel phenomenon could be observed under shorter and stronger laser pulse. In terms of theoretical studies, this may lead to the adoption of the more sophisticated simulation program in order to capture the essential physics beyond the drift-diffusion model. Hence, the further studies are highly expected in both experimental and theoretical aspects.

5. Acknowledgment

The authors acknowledge the financial support from the National Natural Science Foundation of China and the National Basic Research Program of China.

6. References

Dekorsy T. ; Auer H. ; Bakker H. J. ; Roskos H. G. & Kurz H. (1996). THz electromagnetic emission by coherent infrared-active phonons, *Phys. Rev. B*, Vol.53, pp. 4005-4014

Dekorsy T.; Pfeifer T.; Kütt W. & Kurz H. (1993). Subpicosecond carrier transport in GaAs surface-space-charge fields, *Phys. Rev. B*, Vol. 47, pp. 3842-3849

Ge C.; Jin K. J.; Lu H. B.; Wang C.; Zhao G. M.; Zhang L. L. & Yang G. Z. (2010). Mechanisms for the enhancement of the lateral photovoltage in perovskite heterostructures. *Solid State Commu.,* Vol.150, pp. 2114-2117

Grasser T.; Tang T. W.; Kosina H. Selberherr S. (2003). A Review of Hydrodynamic and Energy-Transport Models for Semiconductor Device Simulation, *Proc. IEEE*, Vol.91, pp. 251

Gu P.; Tani M.; Kono S.; Sakai K. & Zhang X.-C. (2002). Study of terahertz radiation from InAs and InSb, *J. Appl. Phys.*, Vol.91, pp. 5533-5537

Han P.; Jin K. J.; Lu H. B.; Zhou Q. L.; Zhou Y. L. & Yang G. Z. (2007). The mechanism study on transport properties in perovskite oxide p-n junction, *Appl. Phys. Lett.*, Vol.91, pp.182102

Henry J. & Livingstone J. (2001). Thin-film amorphous silicon position-sensitive detectors, *Adv. Mater.*, Vol.13, pp. 1-4

Hu C. L.; Jin K. J.; Han P.; Lu H. B.; Liao L. & Yang G. Z. (2008). The effect of phase separation on the temperature dependent magnetoresistance in perovskite oxide heterojunction, *Appl. Phys. Lett.*, Vol.93, pp.162106

Hu C. L.; Jin K. J.; Han P.; Lu H. B.; Liao L. & Yang G. Z. (2009). Theoretical study on the positive magnetoresistance in perovskite oxide p-n junctions, *Solid State Commun.*, Vol.149, pp.334

Huang Y. H.; Jin K. J.; Zhao K.; Lu H. B.; He M.; Chen Z. H.; Zhou Y. L.; Yang G. Z. & Ma X. L. (2006). Photoelectric Characteristic of $La_{0.9}Sr_{0.1}MnO_3/SrNb_{0.01}Ti_{0.99}O_3$ p-n Heterojunctions, *Chin. Phys. Lett.*, Vol.23, pp. 982

Jain R. K. & Landis G. A. (1998). Transient response of gallium arsenide and silicon solar cells under laser pulse, *Solid-State Electron.*, Vol.42, pp. 1981-1983

Jin K. J.; Lu H. B.; Zhao K.; Ge C.; He M. & Yang G. Z. (2009). Novel Multifunctional Properties Induced by Interface Effects in Perovskite Oxide Heterostructures. *Adv. Mater.*, Vol.21, pp. 4636-4640

Jin K. J.; Zhao K.; Lu H. B.; Liao L. & Yang G. Z. (2007). Dember effect induced hotovoltage in perovskite p-n heterojunctions, *Appl. Phys. Lett.*, Vol.91, pp. 081906

Krotkus A. (2010). Semiconductors for terahertz photonics applications, *J. Phys. D: Appl. Phys.*, Vol. 43, pp. 273001

Liao L.; Jin K. J.; Ge C.; Hu C. L.; Lu H. B. & Yang G. Z. (2010). A theoretical study on the dynamic process of the lateral photovoltage in perovskite oxide heterostructures. *Appl. Phys. Lett.*, Vol.96, pp. 062116

Liao L.; Jin K. J.; Han P.; Zhang L. L.; Lu H. B. & Ge C. (2009a). Acceptor Concentration Effects on Photovoltaic Response in the $La_{1-x}Sr_xMnO_3/SrNb_yTi_{1-y}O_3$ Heterojunction, *Chin. Phys. Lett.*, Vol.26, pp. 057301

Liao L.; Jin K. J.; Lu H. B.; Han P.; He M. & Yang G. Z. (2009b). Dynamic process of photovoltaic effect in $La_{0.9}Sr_{0.1}MnO_3/SrNb_{0.01}Ti_{0.99}O_3$ heterojunction, *Solid State Commu.,* Vol.149, pp. 915-918

Liao L.; Jin K. J.; Lu H. B.; Qiu J.; Han P. & Zhang L. L. (2009c). Theoretical study on the photodoping effects in $La_{1-x}Sr_xMnO_3/SrNb_yTi_{1-y}O_3$ p–n heterojunction, *Phys. Status Solidi A*, Vol.206, pp. 1655-1659

Liu K.; Xu J. Z.; Yuan T. & Zhang X.-C. (2006). Terahertz radiation from InAs induced by carrier diffusion and drift, *Phys. Rev. B*, Vol.73, pp. 155330

Lu H. B.; Jin K. J.; Huang Y. H.; He M.; Zhao K.; Cheng B. L.; Chen Z. H.; Zhou Y. L.; Dai S. Y. & Yang G. Z. (2005). Picosecond photoelectric characteristic in $La_{0.7}Sr_{0.3}MnO_3$/Si p-n junctions, *Appl. Phys. Lett.*, Vol.86, pp. 241915

Lucovsky G. (1960). Photoeffects in nonuniformly irradiated p-n junction, *J. Appl. Phys.*, Vol.31, pp. 1088

Lv X.; Huang Y.; Liu Z. B.; Tian J. G.; Wang Y.; Ma Y.; Liang J. J.; Fu S. P.; Wan X. J. & Chen Y. S. (2009). Photoconductivity of Bulk-Film-Based Graphene Sheets, *Small*, Vol. 5, pp. 1682

Ohtomo A. & Hwang H. Y. (2004). A high-mobility electron gas at the $LaAlO_3/SrTiO_3$ heterointerface, *Nature*, Vol.427, pp. 423

Pankove J. I. (1971). *Optical Processes in Semiconductors,* Prentice-Hall, Englewood Cliffs, New Jersey, U.S.

Qiu J.; Lu H. B.; Jin K. J.; He M. & Xing J. (2007). Manganite-layer thickness-dependent photovoltaic effect of $La_{0.9}Sr_{0.1}MnO_3/SrNb_{0.01}Ti_{0.99}O_3$ p-n heterojunction, *Physica B*, Vol.400, pp. 66-69

Reyren N.; Thiel S.; Caviglia A. D.; Kourkoutis L.; Hammerl G.; Richter C.; Schneider C. W.; Kopp T.; Rüetschi A. S.; Jaccard D.; Gabay M.; Muller D. A.; Triscone J. M. & Mannhart J. (2007). Superconducting Interfaces Between Insulating Oxides, *Science*, Vol.317, pp. 1196

Scharfetter D. L. and Gummel H. K. (1969). Large-signal analysis of a silicon read diode oscillator, *IEEE Trans. Electron Devices*, Vol.ED-16, pp. 64–77

Selberherr S. (1984). *Analysis and Simulation of Semiconductor Devices*, Springer-Verlag, Wien, New York

Shockley W. & Read W. T. (1952). Statistics of the Recombinations of Holes and Electrons, *Phys. Rev.*, Vol.87, pp. 835

Sun J. R.; Xiong C. M.; Shen B. G.; Wang P. Y. & Weng Y. X. (2004). Manganite-based heterojunction and its photovoltaic effects, *Appl. Phys. Lett.*, Vol.84, pp. 2611-2613

Sun J. R.; Xiong C. M.; Shen B. G.; Wang P. Y. & Weng Y. X. (2004). Manganite-based heterojunction and its photovoltaic effects, *Appl. Phys. Lett.*, Vol.84, pp. 2611

Tonouchi M. (2007). Cutting-edge terahertz technology, *Nat. Photonics*, Vol.1, pp. 97-105

Wallmark J. T. (1957). A new semiconductor photocell using lateral photoeffect, *Proc. IRE*, Vol.45, pp. 474

Wen J.; Jin K. J.; He M.; Lu H. B.; Yang F. & Yang G. Z. (2009). The substrate thickness dependence of the photovoltage in $LaAlO_{3-\delta}$/Si heterostructures, *Appl. Phys. Lett.*, Vol.94, pp. 061118

Yan Z. J.; Yuan X.; Xu Y. B.; Liu L. Q. & Zhang X. (2007). Photovoltaic effects in obliquely deposited oxygen-deficient manganite thin film, *Appl. Phys. Lett.*, Vol.91, pp. 104101

Yang G. Z.; Lu H. B.; Chen F.; Zhao T. & Chen Z. H. (2001). Laser molecular beam epitaxy and characterization of perovskite oxide thin films, *J. Cryst. Growth.*, Vol.227-228, pp. 929-935

Yang K.; East J. R. & Haddad G. I. (1993). Numerical modeling of abrupt heterojunctions using a thermionic-field emission boundary condition, *Solid State Electron.*, Vol.36, pp. 321

Yu C. Q. & Wang H. (2010). Light-induced bipolar-resistance effect based on metal-oxide-semiconductor structures of Ti-SiO_2-Si, *Adv. Mater.*, Vol.22, pp. 966–970

Zhang P. X.; Lee W. & Zhang G. Y. (2002). Time dependence of laser-induced thermoelectric voltages in $La_{1-x}Ca_xMnO_3$ and $YBa_2Cu_3O_{7-\delta}$ thin films, *Appl. Phys. Lett.*, Vol.81, pp. 4026

Zhao K.; Huang Y. H.; Zhou Q. L.; Jin K. J.; Lu H. B.; He M.; Cheng B. L.; Zhou Y. L.; Chen Z. H. & Yang G. Z. (2005). Ultraviolet photovoltage characteristics of $SrTiO_{3-\delta}$/Si heterojunction, *Appl. Phys. Lett.*, Vol.86, pp. 221917

Zhao K.; Jin K. J.; Huang Y. H.; Lu H. B.; He M.; Chen Z. H.; Zhou Y. L. & Yang G. Z. (2006a). Laser-induced ultrafast photovoltaic effect in $La_{0.67}Ca_{0.33}MnO_3$ films at room temperature, *Physica B,* Vol.373, pp. 72-75

Zhao K.; Jin K. J.; Huang Y. H.; Zhao S. Q.; Lu H. B.; He M.; Chen Z. H.; Zhou Y. L. & Yang G. Z. (2006b). Ultraviolet fast-response photoelectric effect in tilted orientation $SrTiO_3$ single crystals, *Appl. Phys. Lett.*, Vol.89, pp. 173507

Zhao K.; Jin K. J.; Lu H. B.; Huang Y. H.; Zhou Q. L.; He M.; Chen Z. H.; Zhou Y. L. & Yang G. Z. (2006c). Transient lateral photovoltaic effect in p-n heterojunctions of La0.7Sr0.3MnO3 and Si, *Appl. Phys. Lett.*, Vol.88, pp. 141914

Zhou Q. L.; Jin K. J.; Lu H. B.; Han P.; Chen Z. H.; Zhao K.; Zhou Y. L. & Yang G. Z. (2005). Transport property in $SrTiO_3$ p-n junction, *Europhys. Lett.*, Vol.71, pp. 283

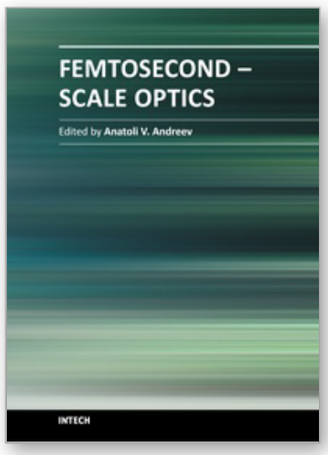

Femtosecond-Scale Optics
Edited by Prof. Anatoly Andreev

ISBN 978-953-307-769-7
Hard cover, 434 pages
Publisher InTech
Published online 14, November, 2011
Published in print edition November, 2011

With progress in ultrashort ultraintense laser technologies the peak power of a laser pulse increases year by year. These new instruments accessible to a large community of researchers revolutionized experiments in nonlinear optics because when laser pulse intensity exceeds or even approaches intra-atomic field strength the new physical picture of light-matter interaction appears. Laser radiation is efficiently transformed into fluxes of charged or neutral particles and the very wide band of electromagnetic emission (from THz up to x-rays) is observed. The traditional phenomena of nonlinear optics as harmonic generation, self-focusing, ionization, etc, demonstrate the drastically different dependency on the laser pulse intensity in contrast the well known rules. This field of researches is in rapid progress now. The presented papers provide a description of recent developments and original results obtained by authors in some specific areas of this very wide scientific field. We hope that the Volume will be of interest for those specialized in the subject of laser-matter interactions.

How to reference
In order to correctly reference this scholarly work, feel free to copy and paste the following:

Kui-juan Jin, Chen Ge, Hui-bin Lu and Guo-zhen Yang (2011). Laser Pulses Applications in Photovoltaic Effect, Femtosecond-Scale Optics, Prof. Anatoly Andreev (Ed.), ISBN: 978-953-307-769-7, InTech, Available from: http://www.intechopen.com/books/femtosecond-scale-optics/laser-pulses-applications-in-photovoltaic-effect

INTECH
open science | open minds

InTech Europe
University Campus STeP Ri
Slavka Krautzeka 83/A
51000 Rijeka, Croatia
Phone: +385 (51) 770 447
Fax: +385 (51) 686 166
www.intechopen.com

InTech China
Unit 405, Office Block, Hotel Equatorial Shanghai
No.65, Yan An Road (West), Shanghai, 200040, China
中国上海市延安西路65号上海国际贵都大饭店办公楼405单元
Phone: +86-21-62489820
Fax: +86-21-62489821

© 2011 The Author(s). Licensee IntechOpen. This is an open access article distributed under the terms of the Creative Commons Attribution 3.0 License, which permits unrestricted use, distribution, and reproduction in any medium, provided the original work is properly cited.

IntechOpen

IntechOpen